Appl Phys B (2009) 95: 825–838
DOI 10.1007/s00340-009-3534-8

Applied Physics B
Lasers and Optics

Soot volume fraction measurements in aero-engine exhausts using extinction-calibrated backward laser-induced incandescence

J. Delhay · P. Desgroux · E. Therssen · H. Bladh · P.-E. Bengtsson · H. Hönen · J.D. Black · I. Vallet

Received: 26 September 2008 / Revised version: 20 March 2009 / Published online: 5 May 2009

Abstract Control and reduction of soot particle emissions from aeronautic turbines requires a monitoring system suitable for quantification of these emissions. Currently, such emissions are estimated using the technique of smoke number. This is an extractive method, which is not sensitive enough for the low emission levels of modern gas turbines. Within a recent European project, AEROTEST, part of the project aimed at investigating an alternative soot monitoring technique, laser-induced incandescence (LII) as an in-situ optical diagnostic for quantification of soot emissions. For aero-engine applications, especially those involving large-scale turbines, it is necessary to perform the measurements at long distance from the turbine. The LII technique is favourable in this respect as it provides for non-intrusive measurements and, by detecting the isotropic LII signal along the same axis as the incoming laser beam (so called backward LII), both the laser and the detector can be built inside one system located several meters from the turbine. The concept was initiated in the previous European projects, AEROJET I and II. This paper describes the modified version of the system and the procedure developed to achieve reliable and quantitative soot volume fraction measurements in the exhausts of aero-engines. Application of the backward LII technique is demonstrated in the exhaust of a military turbojet engine for different engine speeds.

PACS 42.62.-b · 42.62.cf · 42.62.Eh

J. Delhay · P. Desgroux (✉) · E. Therssen
Physico-Chimie des Processus de Combustion et de l'Atmosphère (PC2A), UMR CNRS 8522, Université des Sciences et Technologies de Lille, Fédération de Recherche "Centre d'Etudes et de Recherches Lasers et Applications", (CERLA), 59655 Villeneuve d'Ascq Cedex, France
e-mail: pascale.desgroux@univ-lille1.fr
Fax: +33-3-20436977

H. Bladh · P.-E. Bengtsson
Division of Combustion Physics, Lund University, P.O. Box 118, 221 00 Lund, Sweden

H. Hönen
Institute of Jet Propulsion and Turbomachinery, RWTH Aachen University, Templergraben 55, 52062 Aachen, Germany

J.D. Black
Rolls–Royce plc, Strategic Research Centre, P.O. Box 31, Derby DE24 8BJ, UK

I. Vallet
Auxitrol S.A., 5 Allée Charles Pathé, 18941 Bourges Cedex, France

1 Introduction

Soot emissions from aircraft engines take place mainly at the troposphere level and have a significant impact on the environment. Soot particles can initiate heterogeneous reactions that modify atmospheric composition [1, 2] and can act as nuclei for ice particle formation [3] leading to contrails. They can also be responsible for the formation of cirrus clouds and can modify radiation transfer [4, 5], all processes that are believed to contribute to climate change. Near ground, epidemiological studies show the responsibility of soot particles in some cancers and respiratory problems due to their small size [6, 7]. Very few data about the mass, number and morphology of soot particles emitted by aero-engines are available [8–10]. A recent morphological study of soot particles issued from aeronautic turbines was performed using transmission electron microscopy (TEM) and scanning electron microscopy (SEM) [10] confirming the small dimension of the emitted particles; primary soot

particles were found to be spherical with a diameter ranging from 10 to 22 nm. In addition to environmental strategies, monitoring emission is a useful indicator of the engine health condition. An increase in soot emission can be an early indication that maintenance intervention is required [11].

The current requirement for certification of aero-engine requires a measurement of smoke number (SAESN) [12]. Exhaust gas is sampled using a rake of probes. Four liters of sampled gas are passed through a filter paper and SAESN is determined from the reflectance of the stained filter paper. This is the slowest step in the emissions certification process. It is also not sensitive enough for measurement of low concentrations of particles emitted by current engines at low power conditions. A promising alternative is Laser-Induced Incandescence (LII), which has emerged as an attractive non-intrusive method for real-time soot volume fraction monitoring in practical devices. The LII technique is based on the detection of increased thermal radiation from soot particles heated to very high temperatures (∼4000 K) by a short laser pulse. It has been shown that the resulting signal is approximately proportional to the soot volume fraction, f_v [13, 14]. The technique has been extensively used in laboratory flames, see for example [15–17], and also in automobile engines [18–20] and sampled automotive exhaust gas [21]. To the authors' knowledge, only two previous studies report soot particle monitoring in the exhaust of aircraft engines using the LII technique. Both studies rely on the collection of the incandescence signal in a backward configuration fulfilling the remote-sensing requirements of aero-engine test beds. Jenkins et al. [22] developed a compact system in which the collection axis forms an angle of 9 degree with respect to the axis of the incoming laser beam (at a wavelength of 1064 nm). The system allows for spatially-resolved measurements and has been calibrated using a soot generator producing carbon particles of about 500 nm. Black [23] also developed a remote-sensing LII system but with both laser and LII collection axes coincident, simplifying scanning of the laser beam across the exhaust plume. The laser beam (at wavelength 1064 nm) was expanded to a diameter ∼70 mm and focused in the plume with a telescope and the LII radiation was collected in the exact opposite direction via a large-dimension dichroic mirror, enabling the incandescence signal to be collected by a CCD camera. This system was very compact and permitted a fast alignment on test beds. The performance of the initial version of the backward LII system was demonstrated for qualitative measurements of soot in several campaigns [24]. However, initial modelling studies showed that calibration of this focused LII system would be problematic, and this paper describes calibration and application of a backward collection system with a collimated beam providing an integrated measurement along the path of the beam through the exhaust plume.

In order to calibrate the backward-LII system in terms of quantitative soot volume fractions, a 40 kW oil-fired heating burner, connected to a chimney, was adapted to burn kerosene in air. The soot is likely to be similar to that produced in an aero-engine, the main differences being that combustion takes place at atmospheric pressure with air at ambient temperature in the burner. In the chimney section where soot particle temperatures approach those of aero-engine exhausts, a calibration cell was implemented. The soot field across the flow was found to be homogeneous on a 10 cm path length, facilitating a relatively straightforward calibration of the spatially-integrated backward-LII technique. The calibration cell was characterised in terms of soot volume fraction using extinction measurements. Theoretical calculations were used to assess the characteristics of the system and allow analysis of the effects of several parameters on the backward LII measurements.

The backward-LII technique has been applied in several aero-engine test beds during this work (European STREP AEROTEST project). Here, the potential of the technique is demonstrated in detail by measuring quantitatively the soot profile across the exhaust plume of a SNECMA ATAR turbojet aircraft engine at RWTH Aachen and the sensitivity and spatial resolution of the technique are discussed.

2 Experimental equipment and model tools

2.1 The LII system

The backward-LII configuration enables collection of the incandescence signal in the opposite direction of the propagation direction of the incident laser beam. The principle of the system is shown in Fig. 1. The laser beam is aligned through the jet exhaust plume, and the resulting incandescence imaged on an ICCD camera in the counter-propagating direction. The backward-LII signal collected by the camera is shown in the inset of Fig. 1 and represents the spatial LII distribution when path-integrated along the laser beam.

When the measurement system was first designed, the laser beam was expanded and focused in the region of interest using a three-lens telescope [23]. In this study, where the aim was to make quantitative measurements, the focused configuration was abandoned in favour of an unfocused configuration. The signal interpretation from a focused configuration is much more challenging than for an unfocused system, since the laser energy absorbed by soot particles in the exhaust plume is dependent not only on the radial spatial profile of the laser (which is near-Gaussian for the system), but also on the distance from the beam focus. Previously we have shown that the non-uniform radial laser energy distribution in the beam favours a broadening of the spatial

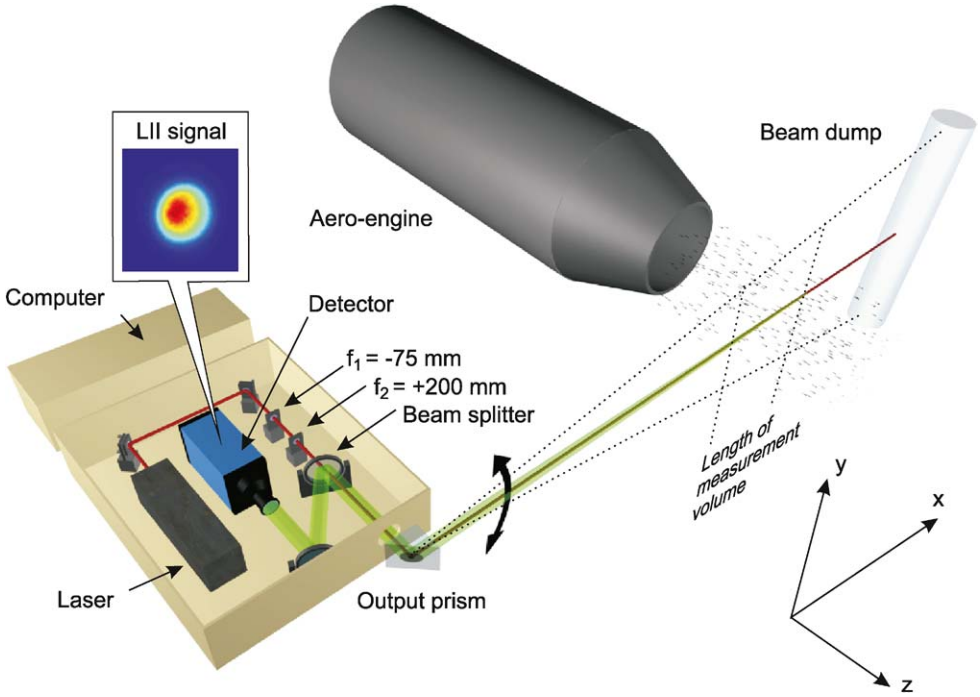

Fig. 1 The experimental setup showing the LII equipment on a test bed to quantify soot particle emissions

LII distribution and a hole-burning effect in the beam centre due to soot sublimation for high laser energies [25, 26]. The focused configuration, where the radial spatial profile varies along the laser beam axis, thus results in a signal averaged over many of these signal contributions. This is illustrated in Fig. 2 for an ideal Gaussian beam profile and propagation in focused and unfocused configuration. Obviously the size and shape of the backward LII signal is a complex function of both laser fluence and soot volume fraction levels along the laser beam. In Fig. 2, showing results for uniform volume fraction and high laser pulse energy, the maximum LII signal does not originate from the focal region and spatial resolution is difficult to estimate. In principle, spatially-resolved measurements are possible for lower pulse energies, but due to the strong dependence of the LII signal on the laser fluence in this fluence regime, quite large uncertainties in calibration are expected if laser fluence, location of focus, etc. is not known. An unfocused configuration was adopted for the new version of the system to simplify signal interpretation and hence system calibration. The objective was to obtain a section of collimated beam over the exhaust plume diameter (typically 0.5 m) located at several meters from the LII system to make it possible to quantify the signal. A compromise had to be made between the laser cross section in the plume (the larger the section, the stronger is the signal) and the local laser fluence (a certain laser fluence must be reached ($\sim$0.20 J/cm^2) in order to make adequate measurements). The set-up described hereafter and illustrated in Fig. 1 has been selected to this aim.

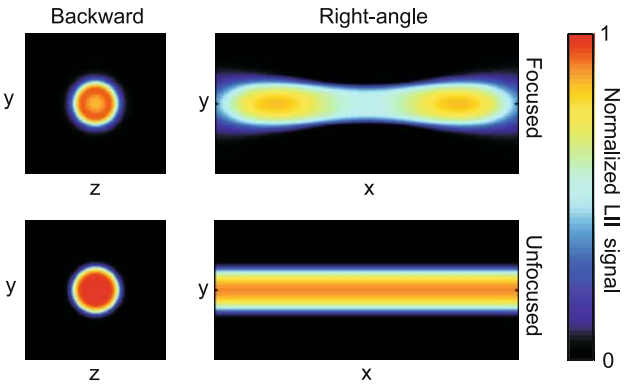

Fig. 2 Modelled backward (*left*) and right-angle (*right*) LII images from focused (*upper* pictures) and unfocused (*lower* pictures) configurations. The coordinate axes are defined in Fig. 1. Note that these signal images are spatially averaged along the third dimension, i.e. the backward along the x-axis and the right angle along the z-axis

The soot diagnostic system is divided into two subsystems: the LII system composed of a shielded box containing laser, detector and collection optics mounted on an optical bench together with a computer to record and store data, and a remote-control system. During the applied measurements, the LII system is located in the aero-engine test bed while the remote-control system is located in the test bed control room. Figure 1 shows the LII system set up for measurements on an engine test bed. It consists of a Nd:YAG laser (Quantel CFR400) operated at 10 Hz emitting pulsed (FWHM $\sim$ 7 ns) radiation at the wavelength 1064 nm. The laser energy can be attenuated using a combination of a polariser and a half-wave plate. The rotation

of this half-wave plate and hence the transmitted laser energy is remotely controlled. The available laser energy at the laser output is 400 mJ and the beam diameter has been estimated to be 9 mm (at $1/e^2$). In order to obtain a laser beam with a near-constant distribution of laser energy along the laser beam axis, a telescope consisting of a diverging lens ($f = -75$ mm) and a converging lens ($f = 200$ mm) is used to compensate the natural divergence of the laser beam. The distance between the lenses is adjusted depending on the distance between the plume and the prism at the laser box output. In most of the experiments the LII system was placed at 2–3 meters from the plume and the beam diameter in the plume was about 7 to 9 mm, giving a maximum peak fluence of about 0.4 J/cm^2. The laser beam emerges from the system via a large right-angle prism, which can be tilted by a stepper motor in order to scan the laser beam through the plume as shown in Fig. 1.

The LII signal is collected through the same scanning prism and reflected by a dichroic mirror and a broadband mirror to a 1280 × 1024 pixels ICCD camera (PCO Dicam Pro, pixel size = 6.7 × 6.7 µm). The detection was not spectrally filtered to get a sufficiently high broadband LII signal on the test beds. However, a filter was placed in front of the camera to block any residual radiation at 1064 nm. Because the signal travels in the opposite direction to the propagation of the incident laser beam, the configuration is termed backward LII. Measurements were performed promptly with a 20-ns gate, to maximise signal and minimise particle size effects. The camera is equipped with a 94 mm UV CERCO camera lens whose aperture can be varied between $f/16$ and $f/2.8$ using a remote-controlled stepper motor. Data was transferred from the camera to the local computer via optical fibre links. The image captured by the camera (inset of Fig. 1) represents the radial LII signal distribution spatially-integrated along the laser beam. The entire LII system is located in the engine test cell and is remote-controlled from the control room with a laptop via an Ethernet connection. The data processing of the LII signal images was performed using Matlab®.

It was observed that the unfocused laser beam generated some visible light when hitting solid surfaces after the measurement region and this stray light interfered with, or even overwhelmed the backward LII image. In smaller engine test cells, for example at RWTH Aachen, it was necessary to terminate the beam in a way that did not generate visible light. A system described in reference [23] was used. A 1.6 m long transparent tube filled with water was placed on the opposite side of the exhaust plume to the LII system as shown in Fig. 1. This functions as a cylindrical lens with very short focal length, bringing the beam to a tight focus just beyond the tube, so that it, when terminated against surfaces, has diverged sufficiently to not generate interfering light. The beam could be scanned along the length of the tube, avoiding the need to translate a beam dump during scanning. In cases where these measures could not completely prevent interferences, a background scan was recorded without the engine running, and background images were subtracted from the LII images in the data analysis. This procedure was found unnecessary in the large test cell at Rolls–Royce, Derby UK, in which the terminating metal surface was ∼9 m from the LII system prism. At that distance the beam had diverged naturally to a diameter >30 mm and did not generate any interference to the LII image [27].

2.2 The calibration system

In order to obtain quantitative soot volume fraction data from the LII system, the system must be calibrated. Calibration using conventional right-angle arrangements usually relies on gravimetric methods [28] or extinction-based measurements [29, 30]. For the latter, laboratory flames are most widely used, but the use of soot generators has also been reported [22]. Recently, the use of an incandescent lamp has been demonstrated for calibration purpose [31]. The latter technique shows to be promising, since it enables calibration without the need of additional sources of soot from flames or soot generators. It relies on absolute intensity calibration of the detectors using an incandescent lamp with well-known irradiance characteristics. For successful results with this approach, it is however essential to have full control of the size of the measurement volume and the optical properties of the soot particles (i.e. the absorption function $E(m)$) must be known. For measurements in aero-engine exhausts using a backward LII approach, where the size of the measurement volume is hard to control due to the non-uniform spatial distribution of the laser energy, and where the optical properties of soot may differ from typical literature values of flame soot, an extinction-based approach in a controlled environment showed more promise as detailed below.

A calibration system has been specially developed to minimise differences in operating conditions for the aero-engine and the calibration system, and it is shown in Fig. 3. A 20–40 kW domestic fuel swirl burner (Weishaupt WL5/1-B) is used to generate the turbulent flames. Domestic fuel was replaced by Jet-A1 kerosene fuel. A kerosene spray is produced through an injector (0.5 Steinen 60°ST). The injection pressure was set to 10 bar and the kerosene mass flow rate was kept constant and equal to 1.5 kg/h. Although not measured, the air flow rate was controlled by setting a flap at the entrance and by measuring the differential pressure (Sensor Technics HCX series 0–10 mbar). In order to produce soot particles and to vary the soot load, the air flow rate was decreased to levels below those encountered in normal domestic use. The burner produces turbulent flames of about 30 cm length and 10 cm in diameter. The

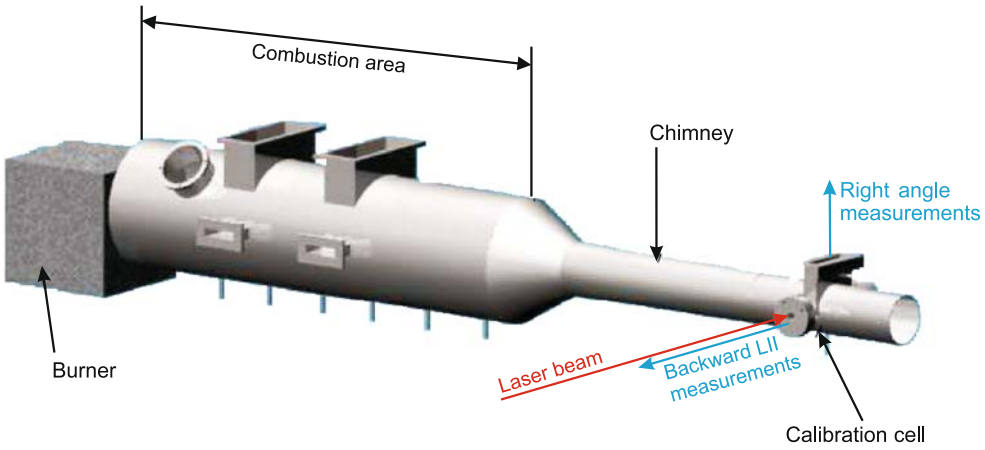

Fig. 3 The calibration burner producing a homogeneous soot field in the calibration cell

combustion system is encircled by a water-cooled cylindrical vessel 30 cm in diameter and 1 m in length. The burnt gases flow though a 12-cm diameter water-cooled chimney. The different parts of the combustion system are equipped with optical access allowing for right-angle and backward LII measurements in both the flame and the exhaust gases. A specially designed calibration cell is located across the chimney 2.3 meters downstream from the burner. As will be shown later, the soot volume fraction levels at this location were found to be nearly homogeneous over a diameter of 10 cm. The homogeneity is important to reduce the uncertainties when comparing the LII signal obtained in the calibration system with the LII signal from the aero-engine plume and integrated over a large diameter (typically 0.5 m). Furthermore the temperature in the calibration cell was probed to be in the range 650 to 850 K using thermocouples, and these temperatures were close to those encountered in the aero-engine exhaust plumes in the test beds.

The calibration relies on right-angle LII, backward LII and extinction measurements (to be described in Sect. 3.1) performed in the calibration cell shown in Fig. 3. The radial soot distribution in the cell was obtained using right-angle LII measurements performed using a second intensified CCD camera (Princeton instruments). In addition, the radial temperature profile was obtained by translating a chromel-alumel thermocouple (type K) across the chimney diameter. Different soot loads were tested by varying the air mass flow rate introduced in the burner, and for all flow rates the LII signal intensity was found to be nearly constant over the cell diameter (12 cm). In Fig. 4, an example is shown for a given air flow rate. The integrated path length (FWHM) is equal to 10.4 cm. Interestingly, the temperature is also nearly constant (750 K) in the same region, see Fig. 4. Lowering the air flow at constant kerosene mass flow rate leads to an increase of the soot load and to a decrease of the burnt

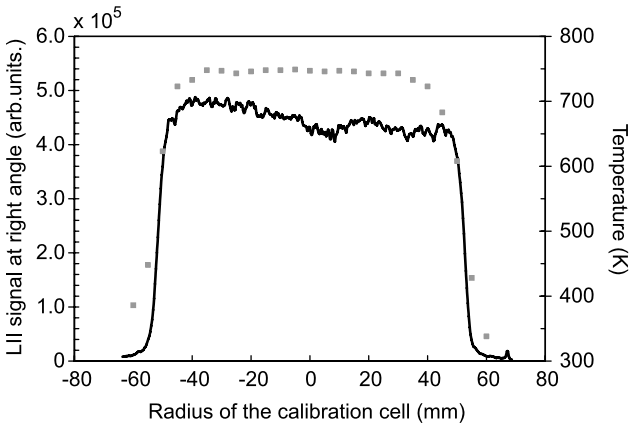

Fig. 4 Radial distributions of the right-angle LII signal (*black curve*) and the temperature (*grey symbols*) obtained in the calibration cell at air flow rate 0.85 (arb. units)

gas temperature, allowing the LII response to be tested over a given range of soot volume fractions.

To summarise, the calibration burner originally developed within this work produces relatively cold soot particles with homogeneous distribution. Using this burner, backward LII measurements can be performed in conditions similar to those on the tests beds, i.e. with a similar distance between the LII system and the burner, similar solid angle etc.

2.3 The LII model

One important tool for the development of the quantitative measurement system is the theoretical model for laser-induced incandescence developed within the project. It is based on a heat and mass transfer model for soot particles exposed to short laser pulses and is fully described elsewhere [14, 32]. The model has the potential to predict both the temporal and spatial signal response from soot particles when using the backward LII configuration. One ex-

ample of this was previously shown in Fig. 2. The model is also capable of predicting the fluence curve from the same systems, enabling direct comparison with measured fluence curves in the calibration cell and on the test beds. Apart from serving as a tool for evaluating various measurement strategies, the model has primarily been used to assess uncertainties involved in providing the quantitative measurements.

3 Calibration procedure

The conversion of an LII signal acquired from an exhaust plume in a test bed into an absolute soot volume fraction (f_v) proceeds as follows. First the relationship between the soot volume fraction obtained from extinction measurements in the calibration cell and backward LII signal yield is established. Then the link between the LII signal obtained in the calibration cell and that measured on a test bed is determined. These steps will be described in this section followed by a discussion of the uncertainties introduced in the procedure.

3.1 Calibration of the backward LII system in the cell

First the soot volume fraction, f_v, in the calibration cell at a given air mass flow rate has been measured using laser extinction according to the Beer-Lambert law, and f_v is calculated as

$$f_v = -\frac{\lambda \ln(I/I_0)}{6\pi E(m) L}, \tag{1}$$

where I is the transmitted laser energy and I_0 the incident one, L the length of the light path through the absorbing medium and $E(m)$ is the absorption function depending on the complex refractive index of soot, m. It has been assumed that soot particles are small enough to be within the Rayleigh limit, i.e. the energy loss due to scattering can be neglected.

Experiments were performed at a wavelength of 1064 nm in the calibration cell. The laser beam was aligned perpendicularly to the exhaust gas flow coming from the kerosene burner (see Fig. 3). The transmitted laser energy was measured using a power meter (Nova, Ophir Optronics). I_0 was measured after the cell but for non-sooting flame conditions to compensate for energy losses in the windows of the cell. The absorption function was assigned the value 0.40 [33] and is discussed in a later part of the paper. From the relatively flat profiles obtained using right-angle LII, the soot volume fraction could be considered homogeneous over a path length of 10.4 cm. Within the available range of air mass flow, attenuation of a few percent were achieved and compared with the backward LII measurements presented hereafter.

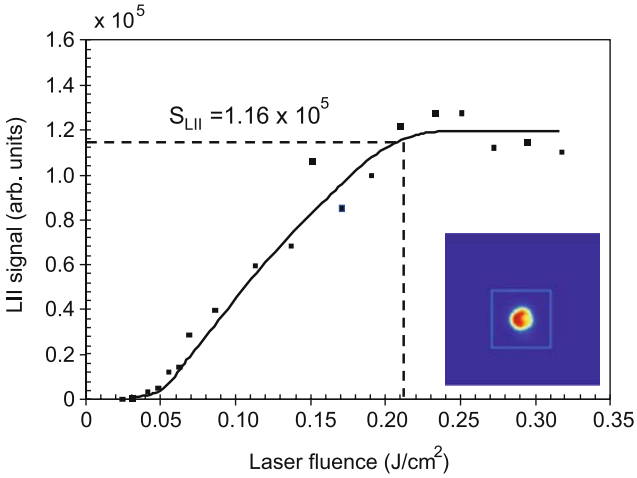

Fig. 5 LII signal as function of the laser fluence. The *inset* represents an image of the backward-LII signal recorded with the camera for a fluence of 0.21 J/cm^2. The *blue square* shows the limits of the region of interest (35 × 35 pixels)

The next step involves calibrating the backward LII system for absolute soot volume fraction. For this purpose the summed pixel intensity from the LII spot was used. A good correlation between backward LII measurements and extinction measurements was found over the f_v range available with the set-up (between 15 and 90 ppb). Calibration was carried out using the following burner conditions: Gas temperature = 750 K and soot volume fraction measured to 44 ppb by extinction. For these calibration conditions, the intensity of the LII signal was recorded as function of the laser fluence as shown in Fig. 5. The shape of this fluence curve is characteristic of a Gaussian beam [34]. The LII signal shows an initial threshold at about 0.03 J/cm^2, after which the signal increases sharply, and at ~0.2 J/cm^2 a region where the LII signal is nearly constant (plateau region) is obtained. The LII signal was recorded promptly during the laser pulse with a gate width of 20 ns. The aperture of the camera lens was $f/8$ and the distance between the LII system output and the calibration cell axis was 2.5 m corresponding to a solid angle of $\Omega = 7 \times 10^{-4}$ sr.

For the calibration procedure, the intensity of the LII signal was chosen just at the beginning of the plateau region for a mean fluence of 0.21 J/cm^2. The LII spot at this fluence is shown in the insert of Fig. 5 and the total intensity of the selected matrix was 1.16×10^5 counts corresponding to a soot volume fraction of 44 ppb (the absorbing length was 10.4 cm). From this calibration step performed in the calibration cell, it is now possible to link the backward-LII intensity to a spatially-integrated soot volume. Extrapolation of this procedure for soot volume fraction determination in aero-engine test beds is detailed below.

3.2 Link between soot volume fraction in the calibration cell and in the exhaust gas of an aero-engine.

The aim of this section is to establish the link between the LII signal measured on a test bed with specific conditions (length of soot volume, distance from the laser, laser fluence, camera aperture, LII signal attenuation, etc.) with the LII signal measured in the calibration cell for corresponding conditions.

The LII system setup on a test bed may differ dependent on the test bed configuration. The LII system is generally placed in a plane containing the plume axis (see Fig. 9 described later), enabling most efficient use of the vertical scanning range of the laser beam. When possible, the LII system is located 2.5 meters from the engine axis i.e. the same distance as during the calibration procedure in the cell. In cases where the distance to the plume differs from 2.5 m, the signal yield will be different due to a change in solid angle. This effect is compensated for by using simple geometrical considerations. The integrated path length L is estimated or assumed to be equivalent to the exhaust plume diameter, which can be measured by scanning through the plume [27]. The other varying parameters of the LII system are (1) the aperture of the camera lens (depending on the intensity of the LII signal) and (2) the laser energy (or laser fluence). The gain of the camera is unchanged during the experiments.

The link between the LII signal measurements in the exhaust plume and the calibration burner is obtained as follows. Consider the local LII signal $S_{\mathrm{LII,Plume}}(x)$ at the position x defined along the laser beam axis in the plume:

$$S_{\mathrm{LII,Plume}}(x) = K\frac{E(m)_{\mathrm{Plume}}}{\lambda_{\mathrm{det}}^6} \times f_v(x)\left[\exp\left(\frac{hc}{\lambda_{\mathrm{det}}kT}\right)-1\right]^{-1}, \tag{2}$$

where K is a calibration constant including the solid angle, the transmission of the set-up (optics, filters, the camera aperture, etc.), $E(m)_{\mathrm{Plume}}$ is the absorption function of soot particles at the detection wavelength, λ_{det} is the detection wavelength of the LII signal, $f_v(x)$ the local soot volume fraction and the term in brackets represents the temperature dependence of the black body radiation from the soot particles. In practical backward-LII applications, the laser beam is aligned perpendicular to the exhaust plume symmetry axis. The backward LII signal integrated along the diameter L_{Plume} of the plume ($\overline{S_{\mathrm{LII,Plume}}}$) is given as

$$\overline{S_{\mathrm{LII,Plume}}} = \int_{L_{\mathrm{Plume}}} S_{\mathrm{LII,Plume}}(x)\,dx = K_{\mathrm{Plume}}\int_{L_{\mathrm{Plume}}} f_v(x)\frac{E(m)_{\mathrm{Plume}}}{\lambda_{\mathrm{det,Plume}}^6} \times \left[\exp\left(\frac{hc}{\lambda_{\mathrm{det,Plume}}kT}\right)-1\right]^{-1} dx. \tag{3}$$

By neglecting the variations of $E(m)_{\mathrm{Plume}}$ within the plume and by assuming that soot particles reach a similar temperature along the x-axis, we can write

$$\overline{S_{\mathrm{LII,Plume}}} = K_{\mathrm{Plume}}\frac{E(m)_{\mathrm{Plume}}}{\lambda_{\mathrm{det,Plume}}^6}\left[\exp\left(\frac{hc}{\lambda_{\mathrm{det,Plume}}kT}\right)-1\right]^{-1} \times \bar{f}_{v,\mathrm{Plume}}L_{\mathrm{Plume}}, \tag{4}$$

where $\bar{f}_{v,\mathrm{Plume}}$ is the mean soot volume fraction integrated along the path of the plume diameter. The assumption of a nearly constant temperature of the heated particles is reasonable along the laser axis because of the use of the unfocused configuration.

In the above equations, we have implicitly considered a monochromatic detection. In practice the LII radiation is collected broadband as detailed in Sect. 2.1. However, including an exact wavelength integration (as was carried out in [26]) in the above equations is unnecessary since only soot volume fraction are deduced from the LII signal. The LII measurements being performed with a short time gate surrounding the laser pulse and with the same detection scheme in the calibration cell and in the plume are relatively independent on the wavelength. It would have been quite different if we were studying particle sizes, where the wavelength-dependent decay-time is used.

Following the same approach used to derive (4) for the test bed, the signal for the calibration cell can be written

$$\overline{S_{\mathrm{LII,Cal}}} = K_{\mathrm{Cal}}\frac{E(m)_{\mathrm{Cal}}}{\lambda_{\mathrm{det,Cal}}^6}\left[\exp\left(\frac{hc}{\lambda_{\mathrm{det,Cal}}kT}\right)-1\right]^{-1} \times \bar{f}_{v,\mathrm{cal}}L_{\mathrm{Cal}}. \tag{5}$$

It is easily seen that the mean soot volume fraction in the plume can be deduced from the comparison between (4) and (5). Provided that the soot particles are heated to the same temperature in the calibration cell and the engine exhausts, the bracketed term is the same in (4) and (5). To obtain this important simplification, our strategy has been (1) to compare the fluence curves obtained in the aero-engine and in the calibration cell, and (2) to heat the soot particles in both cases with the laser fluence required to be just below the plateau region of each fluence curve. Following this approach, the peak temperature is likely to be similar and the expression within brackets will be equal in (4) and (5). Keeping all the experimental parameters constant, one can derive

$$\bar{f}_{v,\mathrm{Plume}} = \bar{f}_{v,\mathrm{Cal}}\left(\frac{L_{\mathrm{Cal}}}{L_{\mathrm{Plume}}}\right)\left(\frac{\overline{S_{\mathrm{LII,Plume}}}}{\overline{S_{\mathrm{LII,Cal}}}}\right) \times \left(\frac{E(m)_{\mathrm{Cal}}}{E(m)_{\mathrm{Plume}}}\right)\left(\frac{K_{\mathrm{Cal}}}{K_{\mathrm{Plume}}}\right). \tag{6}$$

3.3 Assessment of uncertainties

The calibration approach developed to obtain quantitative soot volume fraction data from aero-engine exhausts is based on several assumptions and in this section we will discuss the most important of these. All measurements on soot using optical techniques require knowledge on its optical properties. For the LII process the absorption characteristics of soot described using the absorption function $E(m)$ will be the most important, previously seen appearing in (2)–(6). Since soot particles may show variations in optical properties dependent on their origin and the physical conditions in their surroundings, the value of $E(m)$ must be either measured or assumed. Literature values on $E(m)$ from flame soot have shown variations in the range 0.2–0.42 [30, 33, 35, 36]. Adopting the value 0.4 as mentioned in Sect. 3.1 thus introduces an uncertainty in the absolute levels of soot volume fraction in the calibration cell by at maximum a factor of ∼2. It is important to note that $E(m)$ is an intrinsic property of soot giving uncertainty to optical techniques applied for quantitative soot measurements, including other means of calibrating LII such as the absolute intensity calibration technique [29]. As the soot volume fraction data from the calibration cell is derived using expressions for the Rayleigh limit, errors may be introduced if the soot particles are large enough to result in non-negligible scattering. Finally the soot distribution must be homogeneous, which was verified using the right-angle LII images (see Fig. 4).

Additional uncertainties are introduced when comparing the LII signals obtained in the calibration cell with those obtained from an aero-engine exhaust plume. Experimental parameters such as the collection angle, spatial profile of the laser energy, filter characteristics, and aperture settings can be corrected for and are thus not considered a problem in this respect. There are, however, a number of other parameters which may introduce uncertainties not so easily accounted for. Firstly it is possible that the physical, chemical and optical properties of the soot in the two systems differ, which may give rise to an unexpected signal response thus introducing errors. Considering once more (6) we can directly see how the ratio between the values of the absorption function in the two systems is introduced. In the case where the laser fluence is kept at the same level in both systems, a difference in optical properties will also affect the maximum temperature of the soot particles (due to the heating not being equally efficient in the two systems), hence questioning the validity of the assumption of equal peak temperatures. A difference in initial temperature of the soot also gives rise to this problem, as particles at lower temperature will need higher laser fluence than particles at higher temperature in order to reach the same peak temperature. This is directly noticeable on the fluence curves from such systems, as illustrated in the model results shown in Fig. 6 for a typical

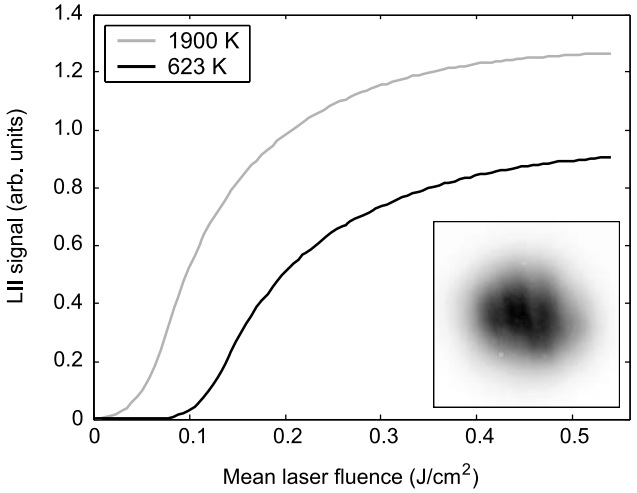

Fig. 6 Modelled fluence curves for a 100 ns gate for the backward LII system using the spatial distribution of the energy of a Quantel Brilliant laser represented in the *inset*. Calculations have been made for both typical flame temperatures and typical gas turbine exhaust temperatures. The particle size is 20 nm

flame temperature and gas turbine exhaust temperature respectively.

In general, these factors may introduce considerable errors in evaluated soot volume fractions, if not corrected for. To give an idea of the size of these errors, the model for LII was used to derive the soot temperature as function of time for two different laser fluence levels. Figure 7 shows the ratio between the expression in brackets in (4) and (5), i.e. the function R:

$$R = \frac{\exp(\frac{hc}{\lambda_{\mathrm{det,Plume}} k T_{\mathrm{Plume}}}) - 1}{\exp(\frac{hc}{\lambda_{\mathrm{det,cal}} k T_{\mathrm{cal}}}) - 1}, \tag{7}$$

when considering that (1) both the soot initial temperature ($T_{\mathrm{g}} = 700$ K) and the detection wavelength ($\lambda_{\mathrm{det}} = 700$ nm) are equal in the two systems and (2) that the laser energy in the plume is 0.30 J/cm^2 while it was 0.33 J/cm^2 in the calibration cell. Figure 7b shows that the function R deviates quite substantially from unity for a minor 10% difference in laser fluence. Using a 20 ns prompt gate (shown in Fig. 7b) would give a relative error on evaluated soot volume fraction around 35%.

Unfortunately the uncertainty in the ratio of the absorption function values and the uncertainty introduced due to different peak temperatures both affect the LII signal response thus making it hard to account for. We here summarise the approach used in this work to minimise the uncertainties.

1. The calibration system has been developed with the aim of providing soot with *properties as close as possible to that of aero-engine soot*. By burning the same fuel

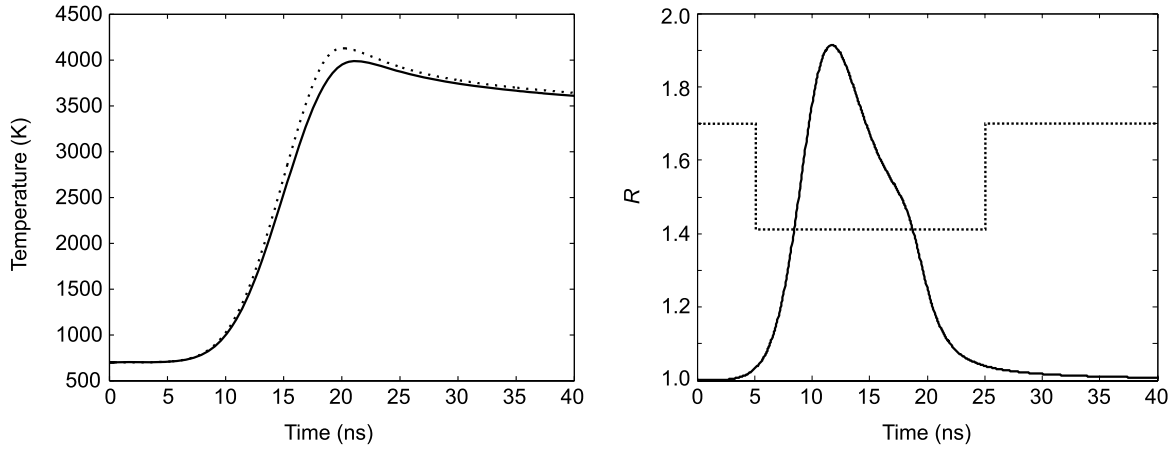

Fig. 7 (**a**) Modelled time-resolved particle temperature for 30 nm particles exposed to a laser fluence of 0.3 J/cm^2 (*solid*) and 0.33 J/cm^2 (*dotted*) respectively, and in (**b**) the ratio R defined in (7) is shown as function of time. The gate of the detector system is indicated

(kerosene) and measure in a homogeneous soot distribution at a similar gas temperature as in the aero-engine exhausts, we have made the best possible effort to minimise the difference in soot properties between the two systems.

2. The gas temperature in the calibration cell is similar to measured values in aero-engine exhausts. Provided that the assumption made in point 1 is true, this means that the particles *will reach the same peak temperature when exposed to the same laser fluence*, thus minimizing the errors associated with a difference in peak temperature previously shown in Fig. 6.
3. Both systems are characterised by recording a fluence curve, i.e. the LII signal as function of the laser fluence. Ideally the two curves should be the same. Differences can be explained either by the assumptions made in point 1 or in point 2 being invalid. The approach used in this work has been to adjust the laser pulse energy to obtain an LII signal *at a specific point on the fluence curve* in both the calibration cell and engine exhaust plume. This would ensure that the peak temperature is similar in both cases (assumption 2 holds), but it will leave the validity of assumption 1 undetermined. This means that (6) holds and the uncertainty comes down to the uncertainty in the ratio of the absorption functions. In most cases encountered in the AEROTEST campaigns, a very good agreement was found between fluence curves obtained in the calibration cell or in test beds, reflecting likely similar physical and optical properties of soot (the initial temperature being quite similar). By contrast a variation of $E(m)$ would certainly lead to a shift of the fluence curves [37], a fact that can mean that the operating laser fluence must be adjusted in order to attain the same soot peak temperature (i.e. be on the same position on the shape of the fluence curve).

Although the sources of uncertainty given above are the most crucial, several others have been considered. One of these is the level of aggregation in the soot studied. The model for LII is capable of predicting the LII signal from aggregates provided that the aggregation can be described by the Rayleigh–Debye–Gans theory for polyfractal aggregates. This is believed to be valid as long as the primary particles and the number of particles per aggregate are not too large [38]; the absorption characteristics will be similar to the case of non-aggregated particles. The aggregation will, however, affect the heat conduction process, primarily responsible for the LII signal decay time. If we consider a test case where the signal is measured from a number of primary particles either in isolated ($N_p = 1$) or aggregated ($N_p > 1$) form, the soot volume fraction will be identical, yet the LII signal will differ. The modelled results are shown in Fig. 8. To give an indication of the typical uncertainties involved, a relative error may be defined as the relative difference in signal strength between $N_p = 500$ and $N_p = 1$ of a 100 ns prompt gate. Calculations indicate the relative errors to be less than 9% for the high-fluence case and less than 20% for the low fluence case. This error will decrease with decreasing gate time, especially for the high-fluence case.

There is one fundamental assumption underlying all extinction-based calibration schemes, and this is the assumed linear relationship between the LII signal and the soot volume fraction. Although this approximation often is motivated, there is a size-dependence influencing the dependence of the LII signal on the soot volume fraction. This effect has been investigated in a recent publication by Bladh et al. [14], where attempts have been made to quantify the uncertainties introduced by this assumption for various experimental conditions. Hence, the error in evaluated soot volume fraction will be minimised by having similar particle sizes in the calibration burner and the aero-engine exhausts.

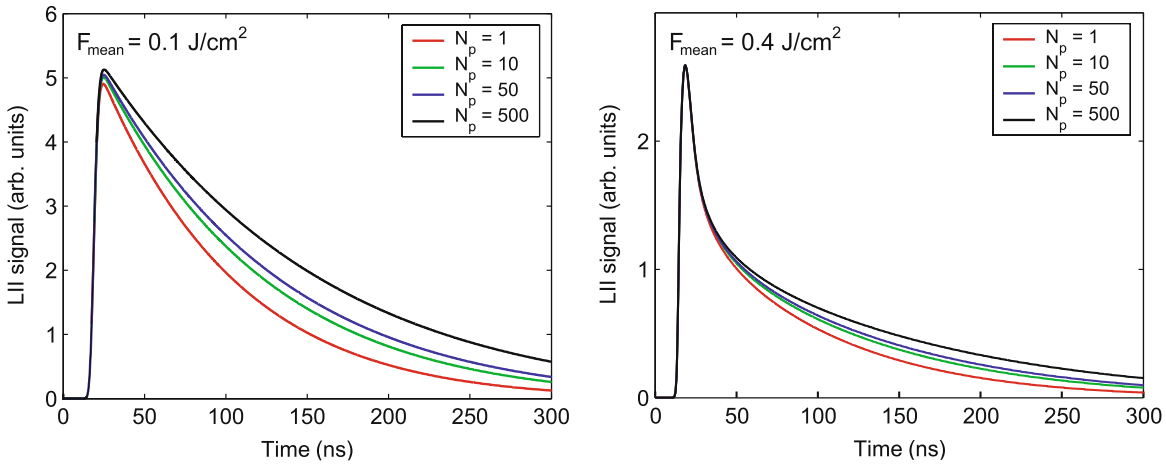

Fig. 8 Modelled LII signals for different level of aggregation for low and high fluence. The calculations have been carried out for a Gaussian beam profile at 1064 nm and detection at 700 nm. The ambient gas temperature is 600 K

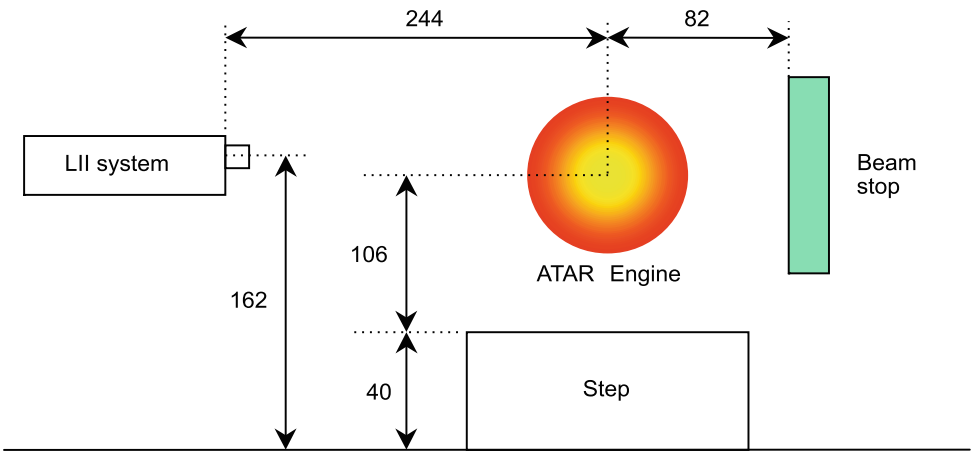

Fig. 9 Configuration of measurement on the ATAR engine (distances are in cm)

4 Measurements

In this chapter the results of a campaign performed in the exhausts of a military turbojet engine turbine (Snecma ATAR 101 F2) available at the University of Aachen (Germany) are presented and discussed.

4.1 ATAR configuration

The ATAR 101F is a SNECMA jet engine with an after burner. In the test bed it is operated in dry mode (with the after burner installed but not operating). The main operating conditions are: thrust 2850 daN, compressor pressure ratio: 4.2, mass flow rate through compressor 52 kg/s, average gas temperature at turbine inlet: 1120 K, average gas temperature at turbine outlet 970 K, and rotor speed 8300 rpm. The engine is equipped with an annular combustor with 20 burners at the circumference. This arrangement provides a quite homogeneous temperature distribution. The engine is installed in a closed test bed with inlet and outlet at ambient conditions. Thus, only investigations at ground conditions are possible. Due to jet effects a large amount of air which has not passed through the engine is entrained into the exhaust duct of the test bed. The total mass flow rate of this air is about 250 kg/s. Downstream of the engine this cold air is mixed with the exhaust stream and leaves the test bed through the exhaust duct. The LII measuring plane was chosen close to the thrust nozzle of the engine so that these mixing effects are negligible. The main parameter which influences the gas temperature at the measuring location is the heat loss over the engine casing downstream of the turbine. The resulting temperature can be estimated to approximately 900 K.

Figure 9 shows the experimental setup for the LII experiments carried out on the ATAR engine at Aachen. The output of the LII equipment was located 2.44 m from the engine centre axis and the laser crossed the plume at 7 cm downstream the engine exhaust nozzle. The laser beam was scanned through the exhaust plume for various engine speeds and various nozzle apertures. The beam dump (de-

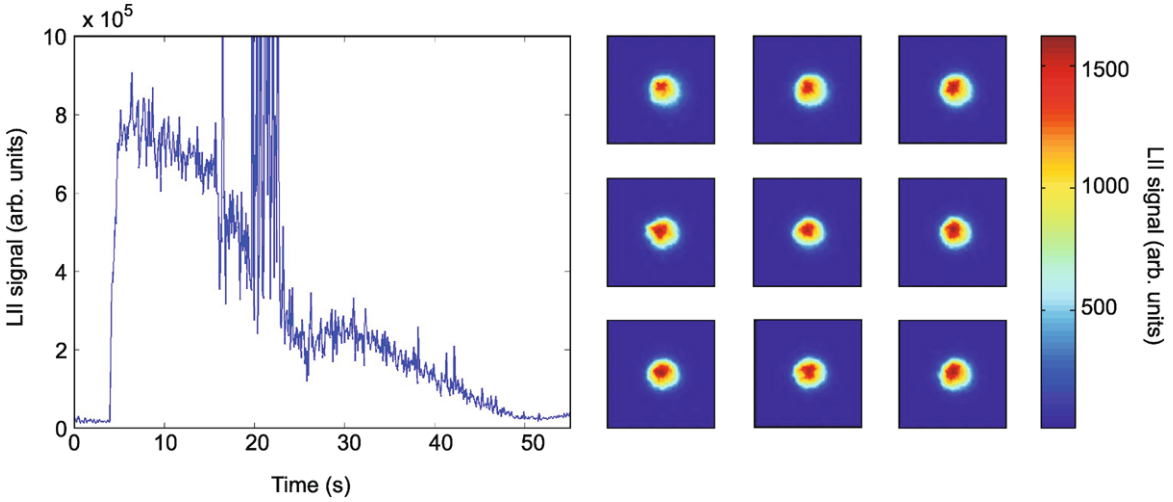

Fig. 10 LII signal (total intensity of the LII spot) measured during the manual start up and examples of single-shot LII spot images

scribed in Sect. 2.1) was located 82 cm from the axis of the engine.

4.2 Results

Most of the measurements have been carried out under steady conditions (either idle, cruise, take-off or thrust). The vertical profile of the LII signal across the plume could be obtained by rotating the output prism of the LII system.

In addition, instantaneous LII measurements were demonstrated during manual start-up of the engine, when large soot loads were produced. An illustration of the single-shot potential of the LII system is illustrated in Fig. 10. The engine is started under manual control. A starter motor accelerates the rotor up to about 600 rpm. At this point kerosene is injected into the 20 burners. Two of them are equipped with heater and spark plugs where the kerosene is evaporated and ignited. After this local ignition the combustion starts to extend over the whole circumference. Now the engine accelerates up to nominal speed by itself. Then the operation is controlled automatically. Since the kerosene is injected in all burners at start up, a large amount of unburned fuel collects at the bottom of the combustion chamber. After the combustion has started this fuel also ignites and forms a large flame front, which passes through the turbine and the thrust nozzle. After a few seconds the waste kerosene is burnt and the combustion chamber can operate normally. During the transient start procedure, LII signals were much higher than at steady engine speed as detailed below.

Experiments were undertaken at different steady engine speeds. Depending on the conditions, the initially circular nozzle can be set elliptic with constant horizontal width ($b = 70$ cm) and decreasing heights (from $h = 70$ to 40 cm).

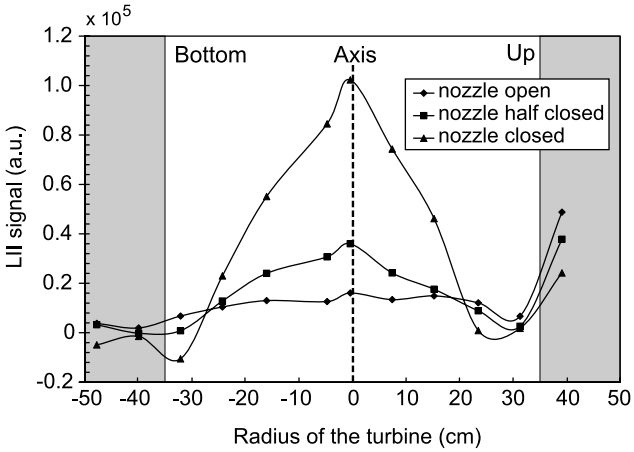

Fig. 11 Profiles of LII signals for three different apertures of the exhaust nozzle

Three regimes have been investigated: take-off with fully open nozzle ($h = 70$ cm), take-off with half-closed nozzle ($h = 55$ cm) and 100% thrust regime with closed nozzle ($h = 40$ cm). The closing of the nozzle led to higher concentration of exhaust gas together with an increase of mass flow rate of kerosene, which induces a higher C/O ratio. Figure 11 represents the variation of the LII signal, path-integrated across the plume, at different heights above the plume axis and measured with a fluence of 0.29 J/cm^2 for three operating conditions (at the idle and cruise regimes, the signal/noise ratio was too low to obtain reliable scans.) Obviously the signal depends on the total path length in the plume which is varying with the angular position of the laser. The reported intensity corresponds to the summation of the intensity of each pixel of the LII spot, to which the summation of the background was subtracted. The plastic

cylinder filled with water, used as a beam dump, was not efficient enough to completely suppress the background signal recorded by the camera. The background signal could vary randomly due to dirt coming on the cylinder during the tests. Grey rectangles on Fig. 11 show the geometrical limits of the exhaust nozzle with open position. A high background signal was recorded above the engine (radius >35 cm) due to visible light generated by the laser beam hitting the metal wall behind the beam dump. At the bottom of the engine the background signal was also high leading to subtraction of inappropriate background levels resulting in a negative net signal.

The results highlight an important effect of the nozzle diameter both on the width of the plume and on the soot emission. The maximum intensity is obtained at the nozzle axis for the three conditions, and the LII signal is nearly symmetrical with respect to the plume axis. As expected, as the nozzle becomes narrower the width of the vertical plume profile decreases and the soot volume fraction increases. The integrated LII signal is found symmetric with the axis of the plume. Tests performed at lower fluence (0.21 J/cm^2) led to similar vertical profiles.

The LII fluence curve, which represents the variation of the LII signal (averaged over 50 laser shots) with laser fluence, was measured to be used for the calibration procedure. Figure 12 compares the fluence curves obtained in the exhaust gas of the turbine and in the burnt gas of the calibration burner under similar experimental conditions (distance between laser and plume, laser beam energy distribution, camera control, etc.). The aperture of the camera was different to take into account the large variation of LII signal between the two experiments. Normalisation was performed at high fluence. It is noteworthy that the shapes of the fluence curves are quite similar. Following the discussion in Sect. 3.3, this indicates that soot particles produced by the kerosene burner and by the aero-engine (burning kerosene) act similarly with regard to the laser fluence. This similar behaviour is interpreted in what follows by considering a constant $E(m)$ in the calibration cell and in the test bed. The last step of the analysis involves calibration of the LII measurements for providing quantitative soot volume fractions. The calibration relies on the comparison of the LII signals, averaged over 50 shots, recorded both in the kerosene burner and in the plume under controlled experimental conditions (laser fluence, distance between laser and plume, aperture, gate position, etc.). Thus, assuming that $E(m)$ is the same in the calibration cell and in the plume, and introducing the known values of the different parameters used in the procedure, the soot volume fraction in the plume $\bar{f}_{v,\mathrm{Plume}}$ is simply determined using (6).

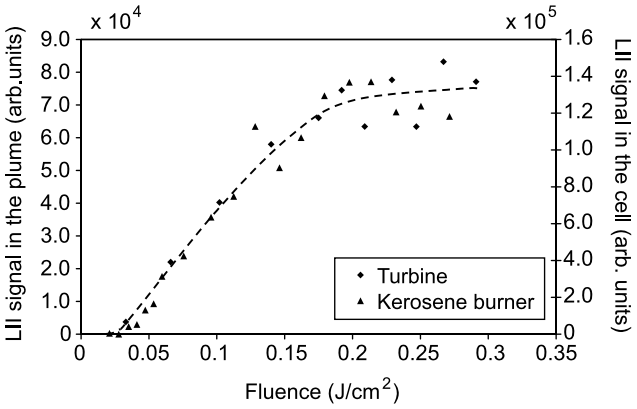

Fig. 12 Fluence curve performed in the calibration cell and in the plume

For each speed, the soot volume fraction on the engine axis, averaged on length $L_{\mathrm{Plume}} = 0.7$ m has been determined as follows: 0.25/0.55/1.55 ppb for open/half-open/close nozzle, respectively. Measurements at idle or cruise regimes were found to be affected by the weak signal/noise ratio (around 1.1–1.2) and led to a soot volume fraction less than 0.1 ppb. Therefore depending on the background fluctuations, variations of the LII signals within a factor of two could be observed. Nevertheless, LII images were recorded at high fluence and the level of soot in the plume could be estimated.

Results are summarised in Fig. 13, which shows the LII images (corrected for background) recorded at different regimes on the engine axis and the corresponding soot volume fraction. From that comparison, and under the experimental conditions in the RWTH test bed, the limit of

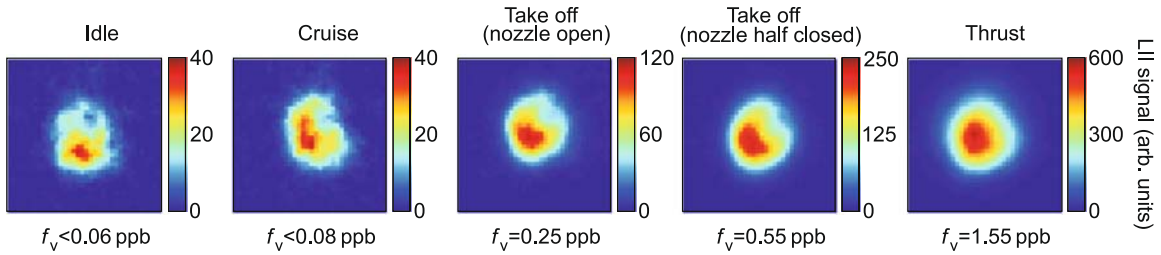

Fig. 13 Soot volume fraction measured with backward LII on the ATAR engine for different speed conditions

sensitivity can be estimated to be 40 ppt. An increase of sensitivity could still be achieved by improving the background rejection.

5 Conclusion

This paper presents the LII system and the procedure specially developed for quantitative measurements of the soot volume fraction in the exhausts of aero-engines. The LII signal is collected counter to the propagation direction of the incident beam (called backward-LII). The LII system has several beneficial properties for use in aero-engine test beds, such as high sensitivity, and capability of remote transient *in-situ* detection. The LII system is also very compact, and easy and fast to implement. Efforts have been concentrated on developing a calibrated and sensitive LII system for aero-engine applications.

The calibration procedure relies on a laboratory-scale soot generator which is able to produce soot from kerosene spray combustion and provides a homogeneous soot field suitable for the backward-LII procedure. Combustion is achieved with a domestic liquid fuel burner connected to a chimney equipped with a cylindrical calibration cell. The radial distributions of soot and temperature in this cell have been found uniform over 10 cm allowing ideal conditions for both laser-extinction and backward LII. The gas temperature is close to that found in the aero-engine test beds (600–900 K). The comparison of extinction with backward-LII has allowed performing an accurate calibration for given settings of the overall experimental parameters of the LII system (laser energy, aperture, solid angle, etc.). The methodology used to calibrate the LII system has been developed using not only experimental considerations, but also theoretical ones. Uncertainties in, for example, gas temperatures and laser fluence have been theoretically analysed in order to estimate their impact on evaluated soot volume fraction data.

Finally, the capabilities of the backward LII system have been demonstrated in the exhausts of an ATAR engine. The system allows for single-shot measurements which are particularly useful to monitor the soot production during transient regimes. Radial profiles of soot volume fractions have been obtained across the plume for different engine regimes. At take-off regime, the soot volume fraction is found to vary from 0.25 to 1.55 ppb depending on the aperture of the turbine nozzle, while idle and cruise regimes produce around 0.1 ppb. The limit of sensitivity has been estimated to be 40 ppt, but may be improved using a more appropriate laser beam dump. Since the end of the AEROTEST programme the calibrated LII system has been used in a large civil aero-engine test bed at Rolls–Royce (Derby, UK) [27] and at Rolls–Royce Deutschland near Berlin. Further improvements will focus on the design of a more compact automated system which will not require a specialist operator.

Acknowledgements This work was supported by Auxitrol S.A. and MEPACA (Pôle capteur, Conseil Régional Centre). The authors thank the European community for financial support of this research under the 6th PCRDT, STREP 502856 AEROTEST. Part of the work by Combustion Physics in Lund was financed by the Swedish Research Council.

References

1. J.T. Houghton, Y. Ding, D.J. Griggs, M. Noguer, P.J. van der Linden, D. Xiaosu (eds.), *Climate Change 2001: The Scientific Basis* (Cambridge University Press, Cambridge, 2001). Contribution of Working Group I to the Third Assessment Report of the Intergovernmental Panel on Climate Change (IPCC)
2. M. Ammann, M. Kalberer, D.T. Jost, L. Tobler, E. Rössler, D. Piguet, H.W. Gäggeler, U. Baltensperger, Nature **395**, 157 (1998)
3. V.H. Grassian, J. Phys. Chem. A **106**, 860 (2002)
4. O. Boucher, Nature **397**, 30 (1999)
5. J.H. Seinfeld, Nature **391**, 837 (1998)
6. E.J. Highwood, R.P. Kinnersley, Environ. Int. **32**, 560 (2006)
7. C. Arden, R.T. Burnett, M.J. Thun, E.E. Calle, D. Krewski, K. Ito, K., G.D. Thurston, J. Am. Med. Assoc. **287**, 1132 (2002)
8. A. Petzold, J. Ström, F.P. Schröder, B. Kärcher, Atmos. Environ. **33**, 2689 (1999)
9. O.B. Popovitcheva, N.M. Persiantseva, M.E. Trukhin, G.B. Rulev, N.K. Shonija, Y.Y. Buriko, A.M. Starik, B. Demirdjian, D. Ferry, J. Suzanne, Phys. Chem. Chem. Phys. **2**, 4421 (2000)
10. D. Delhaye, E. Ruiz, D. Ferry, B. Demirdjian, J. Suzanne, O. Penanhoat, J. Gouge, G. Rollin, Physico-chemical characterization of soot emitted by a commercial aircraft engine: morphology, size, structure, and elemental composition, in *Proceedings of the International Conference on Transport, Atmosphere, and Climate TAC 2006; Office for Official Publications of the European Community*, pp. 22–26, ISBN 92-79-04583-0
11. L.C. Jaw, Recent advancements in aircraft engine health management (EHM) technologies and recommendations for the next step, in *50th ASME International Gas Turbine & Aeroengine Technical Congress* (2005)
12. Aerospace Recommended Practice, SAE ARP1179. Aircraft gas turbine engine exhaust smoke measurement, Rev. C (Society of Automotive Engineers, Warrendale, PA, 1997)
13. L.A. Melton, Appl. Opt. **23**, 2201 (1984)
14. H. Bladh, J. Johnsson, P.-E. Bengtsson, Appl. Phys. B **90**, 109 (2008)
15. C.R. Shaddix, K. Smyth, Combust. Flame **107**, 418 (1996)
16. S. Will, S. Schraml, A. Leipertz, Proc. Combust. Inst. **26**, 2277 (1996)
17. P. Desgroux, X. Mercier, B. Lefort, R. Lemaire, E. Therssen, J.F. Pauwels, Combust. Flame **155**, 289 (2008)
18. J.E. Dec, A.O. zur Loye, D.L. Siebers, SAE Technical paper 910224 (1991)
19. B. Bougie, L.C. Ganippa, A.P. van Vliet, W.L. Meerts, N.J. Dam, J.J. ter Meulen, Combust. Flame **145**, 635 (2006)
20. B.F. Kock, B. Tribalet, C. Schulz, P. Roth, Combust. Flame **147**, 79 (2006)
21. D. Kawano, T. Kawai, H. Naito, Y. Goto, M. Odaka, W.D. Bachalo, SAE Trans. **113**, 1339 (2004)
22. T.P. Jenkins, J.L. Bartholomew, P.A. DeBarber, P. Yang, J.M. Seitzman, R.P. Howard, AIAA paper 2002-3736 (2002)

23. J.D. Black, Laser induced incandescence measurements of particles in aero-engine exhausts, in *Proceedings of the 1999 Environmental Sensing and Applications*, vol. 3821 (1999), pp. 209–215
24. K. Schäfer, J. Heland, D.H. Lister, C.W. Wilson, R.J. Howes, R.S. Falk, E. Lindermeir, M. Birk, G. Wagner, P. Haschberger, M. Bernard, O. Legras, P. Wiesen, R. Kurtenbach, K.J. Brockmann, V. Kriesche, M. Hilton, G. Bishop, R. Clarke, J. Workman, M. Caola, R. Geatches, R. Burrows, J.D. Black, P. Herve, J. Vally, Appl. Opt. **39**, 441 (2000)
25. J. Delhay, Y. Bouvier, E. Therssen, J.D. Black, P. Desgroux, Appl. Phys. B **81**, 181 (2005)
26. H. Bladh, P.-E. Bengtsson, J. Delhay, Y. Bouvier, E. Therssen, P. Desgroux, Appl. Phys. B **83**, 423 (2006)
27. J.D. Black, J. Delhay, M.P. Johnson, P. Desgroux, In-situ laser-induced incandescence of soot in large civil aero-engine exhausts, in *26th AIAA Aerodynamic Measurement Technology and Ground Testing Conference*, 23–26 June 2008, Seattle, USA
28. M.Y. Choi, G.W. Mulholland, A. Hamins, T. Kashiwagi, Combust. Flame **102**, 161 (1995)
29. J.F. Widmann, J. Duchez, J.C. Yang, J.M. Conny, G.W. Mulholland, J. Aerosol Sci. **36**, 283 (2005)
30. T.C. Williams, C.R. Shaddix, K.A. Jensen, J.M. Suo-Antila, Int. J. Heat Mass Transf. **50**, 1616–1630 (2007)
31. D.R. Snelling, G.J. Smallwood, F. Liu, O.L. Gülder, W.D. Bachalo, Appl. Opt. **44**, 6773 (2005)
32. H. Bladh, On the use of laser-induced incandescence for soot diagnostics: from theoretical aspects to applications in engines. Doctoral thesis, Department of Physics, Lund (2007)
33. D.R. Snelling, F. Liu, G.J. Smallwood, Ö.L. Gülder, Combust. Flame **136**, 180 (2004)
34. H. Bladh, P.-E. Bengtsson, Appl. Phys. B **78**, 241 (2004)
35. S.S. Krishnan, K.C. Lin, G.M. Faeth, J. Heat Transf. **123**, 331 (2001)
36. C. Schulz, B.F. Kock, M. Hofmann, H. Michelsen, S. Will, B. Bougie, R. Suntz, G. Smallwood, Appl. Phys. B **83**, 333 (2006)
37. E. Therssen, Y. Bouvier, C. Schoemaecker-Moreau, X. Mercier, P. Desgroux, M. Ziskind, C. Focsa, Appl. Phys. B **89**, 417 (2007)
38. T.L. Farias, Ü.Ö. Köylü, M.G. Carvalho, Appl. Opt. **35**, 6560 (1996)